COMPUTATIONAL IDENTIFICATION OF SELECTED BIOACTIVE COMPOUNDS FROM *CEDRUS DEODARA* AS INHIBITORS AGAINST SARS-COV-2 MAIN PROTEASE: A PHARMACOINFORMATICS STUDY

Aminabee Shaik[a]* and Lakshmana Rao Atmakuri[a]

(Received 19 January 2023) (Accepted 25 January 2024)

ABSTRACT

Amid the ongoing Covid-19 pandemic, the quest for potent antiviral treatments intensifies. This study focuses on the potential of bioactive compounds from the Himalayan cedar *Cedrus deodara* against the SARS-CoV-2 virus. Specifically targeting the main protease (M^{Pro}) and spike protein, the study employs docking trials and molecular dynamics simulations. Compounds such as quercetin, dihydrodehydrodiconiferyl alcohol, and cedeodarin exhibit notable binding affinity, surpassing the reference drug favipiravir. Molecular dynamics simulations affirm the stability of these complexes throughout the simulation period. While these findings underscore promising interactions, it is crucial to emphasize the need for further research and experimental validation to fully explore the therapeutic capabilities of *C. deodara* in combatting Covid-19.

Keywords: *Cedrus deodara,* SARS-CoV-2, remdesivir, quercetin, dihydrodehydrodiconiferyl alcohol, cedeodarin

INTRODUCTION

The global consequences of the ongoing COVID-19 pandemic, attributed to the flinty acute respiratory syndrome corona virus 2 (SARS-CoV-2), have been drastic, leading to the loss of 500,000 lives and 10 million confirmed cases being reported worldwide[1]. Initially identified in late 2019 in the Chinese province of Hubei, the novel corona virus quickly led to a significant rise in cases of atypical pneumonia. Despite significant attempts to control the initial emergence, SARS-CoV-2 has rapidly disseminated, transforming into a worldwide health emergency. It is worth noting that this is the 3rd significant corona virus insurgence in the 21st century, following the 2002 SARS epidemic and the 2012 MERS outbreak[2].

In distinctiveness to the highly infectious and virulent SARS-CoV, SARS-CoV-2 and MERS-CoV there are four additional corona viruses, namely HCoV-HKU1, HCoV-OC43, HCoV-NL63 and HCoV-229E, which are also capable of infecting humans. However, these particular viruses typically result in mild respiratory ailments that resemble common cold symptoms.

As a reaction to the ongoing COVID-19 pandemic, extensive global efforts have been made to swiftly develop vaccines and effective antiviral medications. The main protease (M^{Pro}, 3CLPro, NSP5) has attracted considerable interest as a potential target within the corona virus due to previous studies, especially in the wake of the initial SARS-CoV outbreak in the early 2000s. In addition to M^{Pro}, other potential targets comprehend the spike protein (S), papain-like protease, NTPase/helicase (NSP13) and RNA-dependent RNA polymerase (RdRp, NSP12), with PL^{Pro} being a component of NSP[3].

It is worth noting that the papain-like protease has the unique ability to recognize the C-terminal region of ubiquitin. This presents a challenge in drug discovery campaigns targeting PLpro, as substrate-derived inhibitors of PLpro have the potential to not only inhibit PLpro itself but also host-cell deubiquitinases. This complicates the development of drugs specifically targeting PLpro[4]. To our current understanding, there is no knowledge of host organism proteases possessing the same substrate specificity as this particular protease.

In sharp contrast, the primary protease M^{Pro}, demonstrates a distinct preference for translocating polypeptide sequences following a glutamine residue, making it an appealing target for therapeutic intervention[5]. This is in contrast to viral proteases such as aspartyl proteases used by the human immunodeficiency virus (HIV) or serine proteases used by the hepatitis C virus

[a] Department of Pharmacology, V. V. Institute of Pharmaceutical Sciences, Gudlavalleru-521 356, Andhra Pradesh, India
*For Correspondence: E-mail: aminaammi786@gmail.com

https://doi.org/10.53879/id.61.02.13859

(HCV), which have been successfully targeted with approved medications. Notably, during the replica process of SARS-CoV-2, a critical step involves the proteolytic dissociation of the overlapping pp1a & pp1ab polyproteins into specific proteins, a function performed by the M^{Pro} enzyme. The main protease (M^{Pro}) takes an afflictive role in the viral replication cycle by facilitating the efficient functioning of essential replication enzymes like RdRp or nsp13, which require prior proteolytic release[6].

The Himalayan cedar, scientifically known as *Cedrus deodara*, is a cedar variety native to the Himalayan mountains[7]. High concentrations of taxifolin can be found in the bark of *C. deodara.* The wood of this cedar species contains various compounds such as cedeodarin (3′,4′,5,6-tetrahydroxy-8-methyl dihydroflavonol), ampelopsin, cedrin, cedrinoside and deodarin. The primary components found in the essential oil extracted from the needles include terpineol (30.2%), linalool (24.47%), limonene (17.01%), anethole (14.57%), caryophyllene (3.14%) and eugenol (2.14%). It also contains isopimaric acid, lignans and himasecolone (phenolic sesquiterpene). Some other compounds discovered in this cedar species are (-)-nortrachelogenin, (-)-matairesinol and a dibenzyl butyrol actollignan. The aromatic inner wood of the cedar is used for making incense, while the essential oil derived from it is obtained through distillation[8]. This essential oil is applied to the feet of horses, cattle, and other animals as an insect repellent due to the tree's repellent properties against insects.

C. deodara plants have been extensively utilized in Ayurvedic medicine since ancient times. This tree offers a wide range of medicinal benefits through its various parts, including the heartwood, leaves, bark, oil, and resin[9]. These components are rich in antioxidants and possess natural sedative properties. They have been known to treat conditions such as epilepsy and neurological disorders effectively. Additionally, they are used for healing skin diseases and wounds, relieving gastrointestinal ailments, addressing arthritis, treating coughs, providing a natural remedy for asthma, controlling fever, managing blood disorders, addressing urinary tract problems, alleviating backache, acting as a uterotonic, aiding in weight control, and treating hair loss or alopecia[10].

MATERIALS AND METHODS

Phytoconstituents data

The active phytoconstituents found in *C. deodara* were sourced from the Indian Medicinal Plants, Phytochemistry, and Therapeutic Database (IMPPAT). This comprehensive database provides valuable information about the specific compounds present in *C. deodara*, which have been recognized for their medicinal properties in traditional medicine[11-12].

Drug likeliness

To acquire phytochemical components from PubChem and evaluate their drug-likeliness, the SwissADME and admetSAR tools were utilized. This involved converting the compound structures into SDF format for analysis and assessment[13].

In silico molecular docking

Computational study

The PDB: 7BUY (COVID-19 main protease), atomic coordinates were acquired from the RCSB Protein Data Bank, and subsequent molecular docking studies were executed utilizing the 7BUY structure. The 3D structure of the COVID-19 main protease (7BUY) is depicted in Fig. 1. The plant constituents derived from *C. deodara* were gathered from literature sources and testimonials.

Fig. 1: 3D Structures of main protease (PDB ID: 7BUY)

Ligand structures preparation

The optimized ligand complexes were obtained by the PubChem database in 3D SDF format. To simplify subsequent analysis, the 3D SDF chemical complexes of the ligands were converted to .pdb format applying the BIOVIA DSV (Discovery Studio Visualizer) software[14-15]. Subsequently, AutoDock Tools (ADT) was employed to open the ligands in .pdb file format, allowing for bond rotation and Gasteiger moderation. The ligand structures in .pdb format were then translated to .pdbqt format using AutoDock Vina. Fig. 2 illustrates the three-dimensional structures of several different ligands[16].

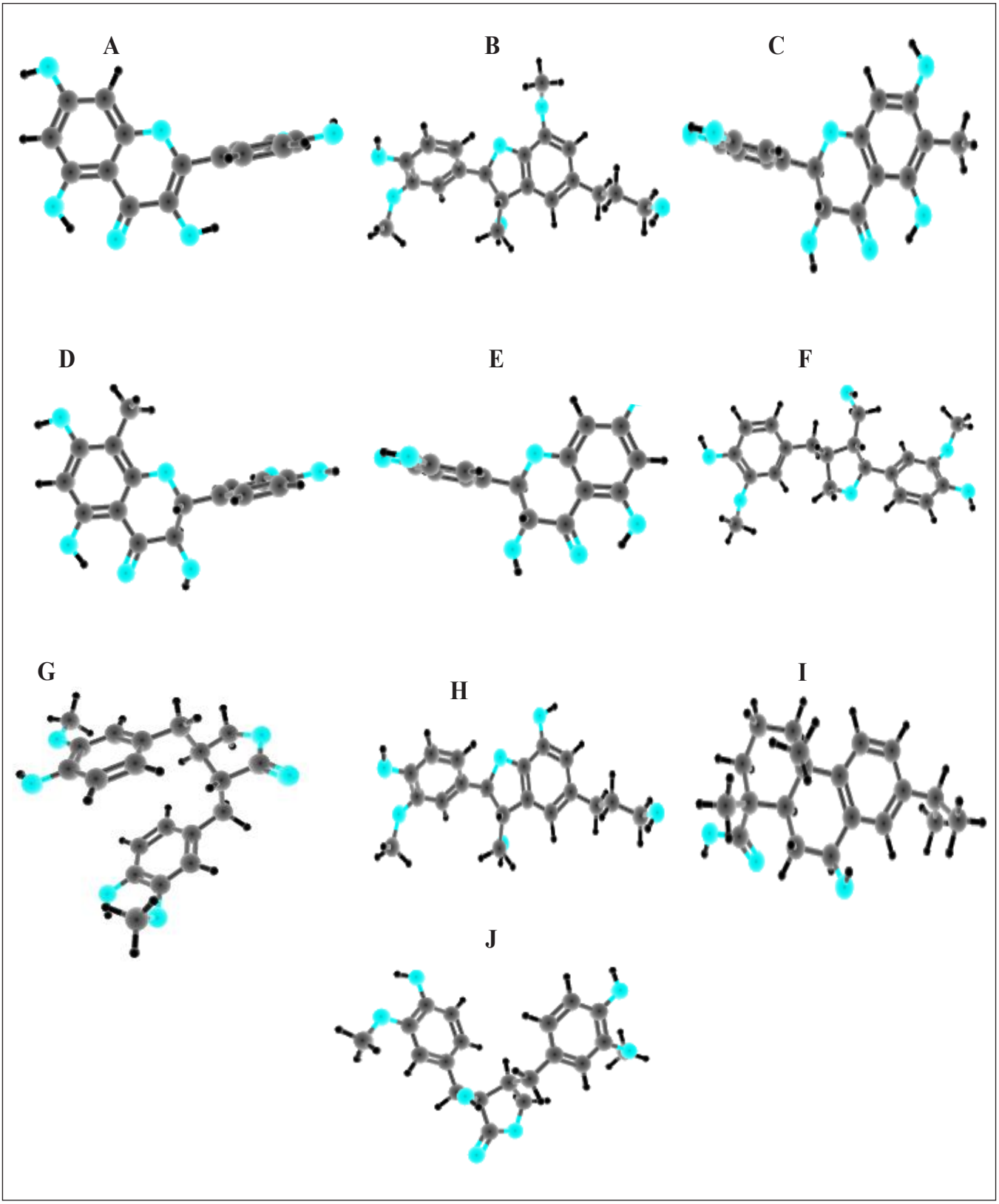

Fig. 2: 3D structures of the ligands utilized in the study A. Quercetin, B. Dihydrodehydrodiconiferyl alcohol, C. Cedeodarin, D. Deodarin, E. Taxifolin, F. Lariciresinol, G. Matairesinol, H. Cedrusin, I. 7-beta-Hydroxydehydroabietic acid and J. Nortrachelogenin

Preparation of COVID-19 main protease

The 3D structure of the major protease of COVID-19 (ID: 7BUY) was obtained by downloading it from the RCSB PDB (Research Collaboratory for Structural Bioinformatics Protein Data Bank). Using BIOVIA Discovery Studio Visualizer, the 7BUY protein structure was opened. H_2O molecules were removed, and the binding sites were defined and modified to reveal the array of ligands within. It was ensured that all ligands were included within the formed binding sphere, which changed color to yellow when clicked and displayed properties such as x, y, and z coordinates when right-clicked[17]. Afterwards, the ligand was eliminated from the structure, and polar hydrogen atoms were incorporated. Once the protein was prepared, it was saved in protein.pdb format. Next, the protein.pdb file was opened in AutoDock Vina, and the grid option for macromolecules was selected. This triggered an initializing pop-up window, following which the file was saved as protein.pdbqt[18].

Active site prediction

Accurately predicting active sites in bioinformatics is an essential process. The estimation of the operating site of the main protease (PDB: 7BUY) was conducted by employing Biovia Drug Discovery Studio Visualizer 2020[19].

Verification of the intricate protein-ligand structures

The validation of the Autodock 4.0 technique involved utilizing co-crystallized ligands that matched the target proteins. This validation ensured the reliability of the simulated screening process. Autodock version 4.0 provides an accurate assessment of target-receptor binding and calculates the RMSD (Root Mean Square Deviation) score[20].

Screening compounds with the Autodock software

During the screening of a molecular compound library by employing Autodock software, the Autodock wizard served as the docking reference. The docking process involved maintaining the protein in a rigid conformation while allowing flexibility for the ligands[21]. To facilitate the docking, a grid criterion configuration file was brought for Autodock, specifying specific proportions (X = -17.521897, Y = 14.973690, Z = 59.408552 for 7BUY). The objective of this study was to identify the amino acids interacting with the ligands at the protein's active site. An ideal Root Mean Square Deviation (RMSD) value below 1.0 was considered, and these values were collectively analyzed to determine the optimal binding relationship. Based on the binding relation of each ligand to the assiduous pocket of the target protein, the most suitable ligand was chosen[22].

Docking methodology

The protein.pdbqt and ligand.pdbqt files were now apt for further analysis. Through various command prompt commands, the complex formed was divided into poses. These poses, along with the protein.pdbqt file, were unfolded in BIOVIA DSV (Discovery Studio Visualizer). By studying the receptor-ligand interrelation, it became possible to determine which pose exhibited the strongest binding affinity with the receptor. The remaining poses that do not display favorable interactions were eliminated[23]. The chosen pose's 2D and 3D structures were captured, and the findings were then interpreted for further analysis and evaluation.

Visualization and analysis

The docking location was visually inspected applying Biovia Drug Discovery Studio 2020, and the obtained data was cross-validated using Autodock Vina[24].

ADMET Analysis

To enhance our understanding on how the ligands function in the body, an ADMET analysis was conducted using admetSAR. This analysis focused on evaluating the pharmacokinetic properties of the ligands. According to Lipinski's Rule of 5 (RO5), a chemical compound can be considered suitable for oral administration in humans as a potential active pharmaceutical ingredient, if it possesses specific physicochemical and pharmacological characteristics[25].

Lipinski's rule of 5 primarily focuses on the pharmacokinetics of drugs, specifically their absorption (A), distribution (D), metabolism (M) and excretion (E) in the human body. However, it does not encompass the pharmacodynamics, which refers to the drug's mechanism of action and its effects on the body. In our work, we utilized the admetSAR and SwissADME tools to assess the ADME (Absorption, Distribution, Metabolism, and Excretion) and toxicological properties of the isolates obtained from *C. deodara*[26]. The SwissADME and admetSAR programs facilitated the ADME/T analysis, and for this analysis, we utilized the canonical smiles representation of the compounds.

Simulation of molecular dynamics

The MD (molecular dynamics) simulations were conducted using GROMACS 2019.4 software with the GROMOS96 force field, as mentioned earlier. All MD simulations were performed on a GPU-enabled workstation[27]. The complexes listed below underwent MD simulations: 7BUY-quercetin, 7BUY-cedeodarin, and 7BUY-favipiravir. The starting point for these simulations was the PDB coordinate file of the protein with the PDB ID 7BUY. In order to ensure a complete and accurate structure, any missing residues in the 7BUY PDB complexes were inserted applying discovery studio.

The preparation of the complexes involved placing it in a 1.0 nm sized cubic box, followed by solvation with H_2O (SPC) and neutralization through the addition of Na^+ ions. The ligand topology file for PDB ID 7BUY in the docked complex MD was generated using the PRODRG2 server configuration. Energy minimization was conducted using the gradient descent algorithm, with 1000 steps performed[28]. Position constraints were applied to keep the 7BUY molecule in place. To achieve equilibration, temperature and pressure equilibration steps were conducted, each lasting for 50,000 ps, with a target of pressure of 1 bar and temperature of 300 K. Following equilibration, MD results were carried out for 50 ns while conserving a pressure of 1 bar and a temperature of 300 K. Plots based on the data from the MD simulations are generated by employing XMGrace software. Additionally, MM-PBSA valuations are executed for the final 20 ns of the different complexes[29].

RESULTS

Characteristics of drug-likeliness

The physicochemical characteristics of 89 selected functional compounds were assessed using the SwissADME and admetSAR tools to analyze their characteristics. The majority of these compounds (excluding 40) complied with Lipinski's rule, as shown in Table I. *C. deodara*'s primary physicochemical characteristics are closely associated with drug absorption, distribution, and permeation.

Table I: Physicochemical characteristics of active molecules and compliance with the drug-likeliness rule

Sr. No.	Ligand	MW (g mol^{-1})	ClogP	Hydrogen acceptors	Hydrogen donors	TPSA (Å²)	MR	Rotatable bonds	Deviations
1.	2,3-Dihydroflavon-3-ol	240.25	2.08	3	1	46.53	66.66	1	0
2.	Quercetin	302.24	1.23	7	5	131.36	78.03	1	0
3.	Deodarin	318.28	0.94	7	5	127.45	79.72	1	0
4.	Juniperol	222.37	3.66	1	1	20.23	68.26	0	0
5.	Taxifolin	304.25	0.63	7	5	127.45	74.76	1	0
6.	Isolariciresinol	360.40	2.02	6	4	99.38	97.33	5	0
7.	Deodarone	236.35	3.04	2	0	26.30	70.88	1	0
8.	Himasecolone	234.33	3.53	2	1	37.30	72.13	5	0
9.	Dihydrode-hydrodiconiferyl alcohol	360.40	2.36	6	3	88.38	96.99	7	0
10.	Cedeodarin	318.28	1.02	7	5	127.45	79.72	1	0
11.	Lariciresinol	360.40	2.38	6	3	88.38	97.09	6	0
12.	meso-Secoisolari-ciresinol	362.42	2.50	6	4	99.38	99.28	9	0
13.	Geranic acid	168.23	2.48	2	1	37.30	51.01	4	0

14.	Malonic acid	104.06	-0.65	4	2	74.60	20.08	2	0
15.	4'-Methylaceto-phenone	134.18	2.19	1	0	17.07	41.60	1	0
16.	7-beta-Hydroxyde-hydroabietic acid	316.43	3.57	3	2	57.53	92.55	2	0
17.	Butyric acid	88.11	0.68	2	1	37.30	23.11	2	0
18.	15-Hydroxyabieta-7,13-dien-18-oic acid	318.45	3.53	3	2	57.53	93.42	2	0
19.	Naringetol	272.25	1.84	5	3	86.99	71.57	1	0
20.	7-beta,18-Dihydroxyde-hydroabietanol	302.45	3.97	2	2	40.46	91.94	2	0
21.	Longiborneol	222.37	3.66	1	1	20.23	68.26	0	0
22.	Santene	122.21	2.83	0	0	0.00	40.67	0	0
23.	Benzyl alcohol	108.14	1.41	1	1	20.23	32.57	1	0
24.	Myrcene	136.23	3.43	0	0	0.00	48.76	4	0
25.	Ascorbic acid	176.12	-1.28	6	4	107.22	35.12	2	0
26.	Spathulenol	220.35	3.26	1	1	20.23	68.34	0	0
27.	Naringetol	272.25	1.84	5	3	86.99	71.57	1	0
28.	4-Carvomenthenol	154.25	2.60	1	1	20.23	48.80	1	0
29.	d-Borneol	154.25	2.38	1	1	20.23	46.60	0	0
30.	Terpinolene	136.23	3.40	0	0	0.00	47.12	0	0
31.	Elemol	222.37	3.77	1	1	20.23	72.10	3	0
32.	gamma-Eudesmol	222.37	3.60	1	1	20.23	70.46	1	0
33.	Camphor	152.23	2.37	1	0	17.07	45.64	1	0
34.	Levomenol	222.37	3.76	1	1	20.23	72.36	4	0
35.	Caryophyllene oxide	220.35	3.68	1	0	12.53	68.27	0	0
36.	Bornyl acetate	196.29	3.00	2	0	26.30	56.33	2	0
37.	Limonene	136.23	3.37	0	0	0.00	47.12	1	0
38.	alpha-Fenchyl alcohol	154.25	2.50	1	1	20.23	46.60	0	0
39.	Himachalol	222.37	3.50	1	1	20.23	70.46	0	0
40.	alpha-Atlantone	218.33	3.99	1	0	17.07	70.88	3	0
41.	Palmitoleic acid	254.41	4.92	2	1	37.30	80.32	13	0
42.	alpha-Terpineol	154.25	2.58	1	1	20.23	48.80	1	0

43.	Allohimachalol	222.37	3.58	1	1	20.23	70.16	0	0
44.	Dihydrodehydro-diconiferyl alcohol	360.40	3.58	6	3	88.38	96.99	7	0
45.	Cedrol	222.37	3.55	1	1	20.23	68.56	0	0
46.	Matairesinol	358.39	2.75	6	2	85.22	96.13	6	0
47.	Cedrusin	346.37	2.04	6	4	99.38	92.52	6	0
48.	Isolariciresinol	360.40	2.02	6	4	99.38	97.33	5	0
49.	Nortrachelogenin	374.38	2.24	7	3	105.45	97.33	6	0
50.	Deodardione	250.33	2.66	3	1	46.53	71.98	1	0
51.	Hexanoic acid	116.16	1.47	2	1	37.30	37.30	4	0
52.	Limonenecarboxylic acid	180.24	2.59	2	1	37.30	53.70	2	0

Studies on molecular docking

A total of 49 phytoconstituents derived from *C. deodara* were subjected to molecular docking analysis in order to recognize a possible candidate against the major protease of COVID-19 (PDB ID: 7BUY, as shown in Fig. 3).

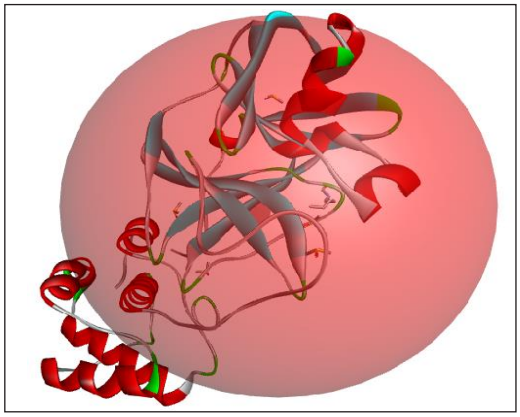

Fig. 3: Prediction of active sites of main protease (PDB ID: 7BUY) by drug discovery Biovia 2020

The 49 phytoconstituents obtained from *C. deodara* were evaluated based on their docking performance with the target enzyme COVID-19. These substances were ranked, and the top three compounds, namely quercetin, dihydrodehydrodiconiferyl alcohol and cedeodarin, demonstrated effective binding to COVID-19 major protease (7BUY) when their dock values for 7BUY interactions were below -7.2 kcal mol^{-1}. Refer Table II for detailed analysis. Based on their binding interactions with 7BUY, these three substances were selected as potential candidates for COVID-19 regulation.

Table II: Molecular docking of specific chemicals with the target protein of the main protease (PDB ID:7BUY)

Sr. No.	Ligand	Docking score (kcal mol^{-1})
1.	Quercetin	-7.2
2.	Dihydrodehydrodiconiferyl alcohol	-7.2
3.	Cedeodarin	-7.2
4.	Deodarin	-7.1
5.	Taxifolin	-7.0
6.	Lariciresinol	-7.0
7.	Matairesinol	-7.0
8.	Cedrusin	-7.0
9.	7-beta-Hydroxyde-hydroabietic acid	-6.9
10.	Nortrachelogenin	-6.9

Research into how molecules interact

Using Discovery Studio, the rigid docking results were utilized for communication analysis. The optimal binding sites for protein-ligand interactions are presented in Table III. The complex of quercetin with the major

Table III: Interactions between the amino acid residues of the COVID-19 Main Protease (PDB ID: 7BUY) and ligands at receptor sites

Compound	Hydrogen binding interaction	Hydrophobic interaction	Electrostatic interactions
Quercetin	ASN A:142, GLY A:143, SER A:144, CYS A:145	MET A:49	
Dihydrode-hydrodiconiferyl alcohol	LEU A:141, GLY A:143, SER A:144, CYS A:145, GLN A:192	HIS A:41, MET A:49	MET A:165
Cedeodarin	ARG A:188, GLN A:192	MET A:49, MET A:165	CYS A:145
Deodarin	LEU A:141, MET A:165, ARG A:188		CYS A:145
Taxifolin	LEU A:141, GLY A:143, SER A:144, CYS A:145, GLU A:166, GLN A:189		MET A:165
Lariciresinol	GLY A:143, GLU A:166, GLN A:189, GLN A:192	HIS A:41	CYS A:145, MET A:165
Matairesinol	GLU A:166	HIS A:41, MET A:49, CYS A:145, HIS A:163	
Cedrusin	LEU A:141, GLY A:143, CYS A:145, GLU A:166, GLN A:192		MET A:165
7-beta-Hydroxyde-hydroabietic acid	GLU A:166	HIS A:41, MET A:49	MET A:165
Nortrachelogenin	HIS A:163, GLU A:166	HIS A:41, MET A:49, MET A:165	CYS A:145

Table IV: ADME/T properties of *C. deodara* compounds

Compound	HIA	BBB	Carcinogenicity	AMES Toxicity
Quercetin	0.9071	0.7750	Non-carcinogenic	Non-toxic
Dihydrodehydrodiconiferyl alcohol	0.9868	0.5750	Non-carcinogenic	Non-toxic
Cedeodarin	0.9215	0.7750	Non-carcinogenic	Non-toxic
Deodarin	0.9215	0.7750	Non-carcinogenic	Non-toxic
Taxifolin	0.9071	0.7750	Non-carcinogenic	Non-toxic
Lariciresinol	0.9186	0.6750	Non-carcinogenic	Non-toxic
Matairesinol	0.9648	0.5250	Non-carcinogenic	Non-toxic
Cedrusin	0.9744	0.5750	Non-carcinogenic	Non-toxic
7-beta-Hydroxydehydroabietic acid	0.9972	0.5250	Non-carcinogenic	Non-toxic
Nortrachelogenin	0.9488	0.5000	Non-carcinogenic	Non-toxic

protease protein exhibited a strong connection with a binding energy of approximately -7.2 kcal mol^{-1}. This complex formed four hydrogen bonds with ASN A:142, GLY A:143, SER A:144, and CYS A:145, as well as one hydrophobic interaction with MET A:49. In the complex of dihydrodehydrodiconiferyl alcohol with the main protease protein, five hydrogen bonds were formed with LEU A:141, GLY A:143, SER A:144, CYS A:145, and GLN A:192, along with two hydrophobic interactions with HIS A:41 and MET A:49, and one sulfur bond with MET A:165. The complex of cedeodarin with the main protease protein formed two hydrogen bonds with ARG A:188 and GLN A:192, 2 hydrophobic interactions with MET A:49 and MET A:165, and 1 sulfur bond with CYS A:145. Please refer to Figs. 4-7 for a visual representation of these interactions.

AdmetSAR use to evaluate ADMET

The ADMET characteristics of the ligands were evaluated using admetSAR, and the results indicate that all the drugs exhibited excellent blood-brain barrier (BBB) penetration and human intestinal absorption (HIA). Additionally, they are found to be non-carcinogenic, and none of the compounds yielded adverse results in the AMES test. Table IV provides a comprehensive overview of the testing results for HIA, BBB, and LD50 of the substances.

Investigations using molecular simulations of 7BUY

To assess the stability of the enzyme or the enzyme-drug complex, Root Mean Square Deviation (RMSD) is commonly employed. In this study, the analysis focused on frames from 10 to 50 ns, revealing that the systems reached an equilibrium state at 50 ns based on RMSD measurements. The systems 7BUY-quercetin, 7BUY-cedeodarin, and 7BUY-favipiravir exhibited average RMSD values of 0.032 nm, 0.037 nm and 0.036 nm, respectively. These values indicate the stability of the compounds throughout the simulation period, as presented in Table V.

Table V: RMSD values of 7BUY-quercetin, 7BUY-cedeodarin, and 7BUY-favipiravir

Time (ns)	RMSD (nm)		
	Quercetin	Cedeodarin	Favipiravir
1	0.0323932	0.0375658	0.0363084
5	0.091300	0.0878046	0.0803703
10	0.1065243	0.097193	0.1036034
15	0.1142081	0.104972	0.1033022
20	0.1093257	0.0960939	0.0849807
35	0.1065243	0.097193	0.1036034
30	0.091300	0.0878046	0.0803703
35	0.1016701	0.1102692	0.1305308
40	0.0901094	0.1256383	0.1274909
45	0.1054995	0.1099615	0.1457931
50	0.0894521	0.1245123	0.8562136

To assess the stability of specific regions, the root mean square fluctuations (RMSF) of the 7BUY-quercetin,

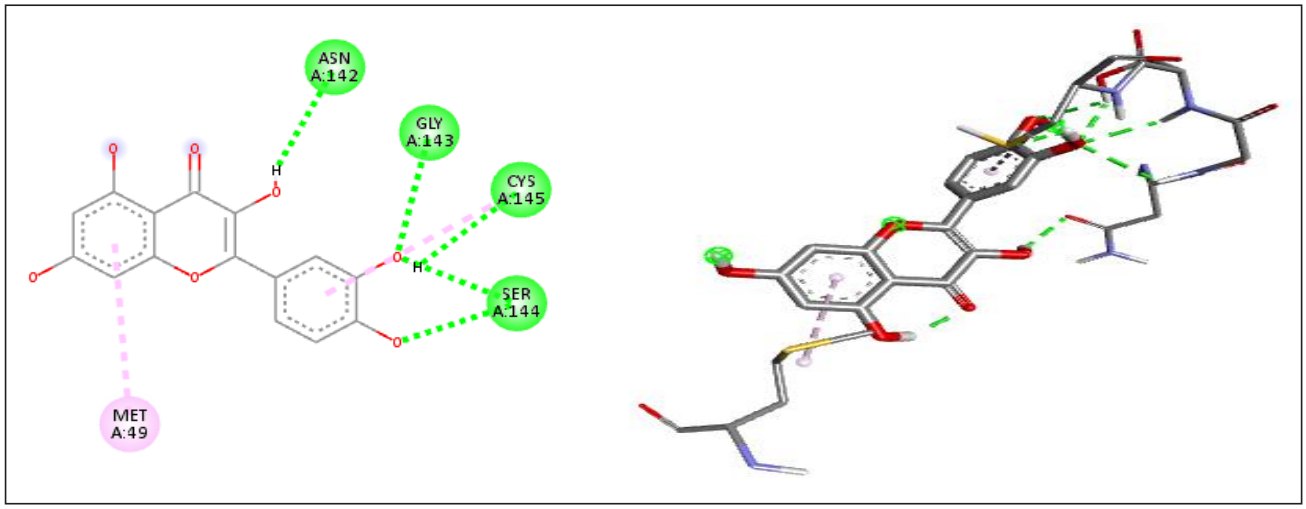

Fig. 4: 2D and 3D interactions of quercetin with main protease (7BUY)

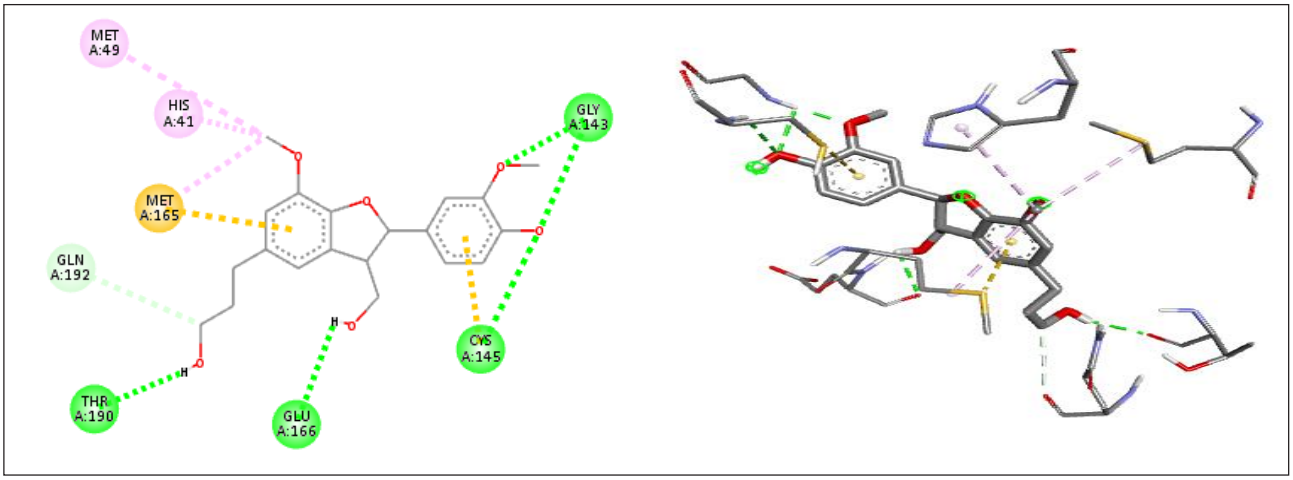

Fig. 5: 2D and 3D interactions of dihydrodehydrodiconiferyl alcohol with main protease (7BUY)

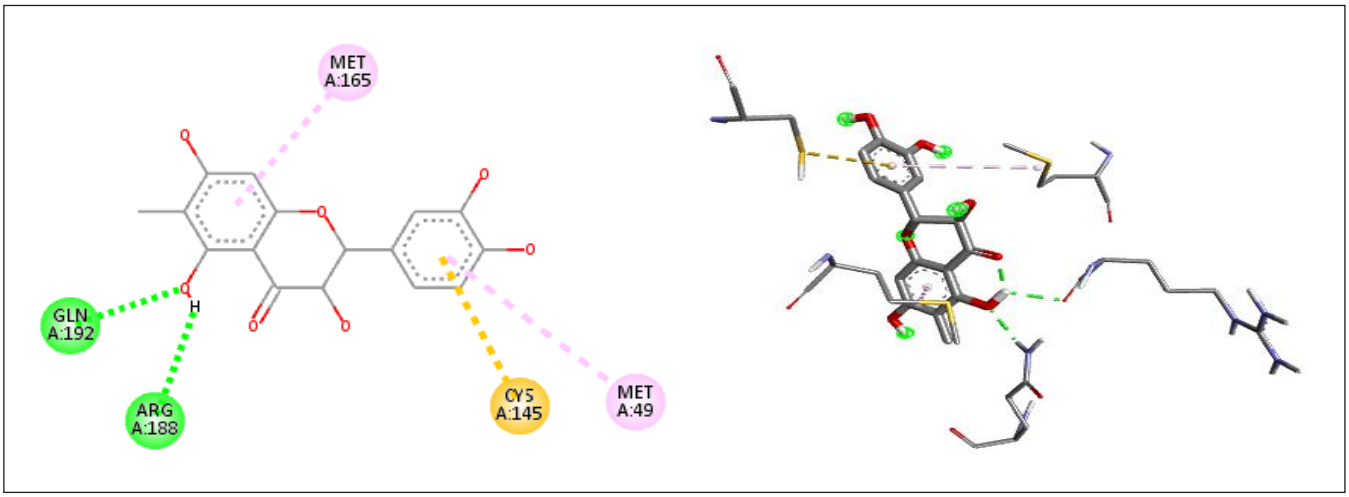

Fig. 6: 2D and 3D interactions of cedeodarin with main protease (7BUY)

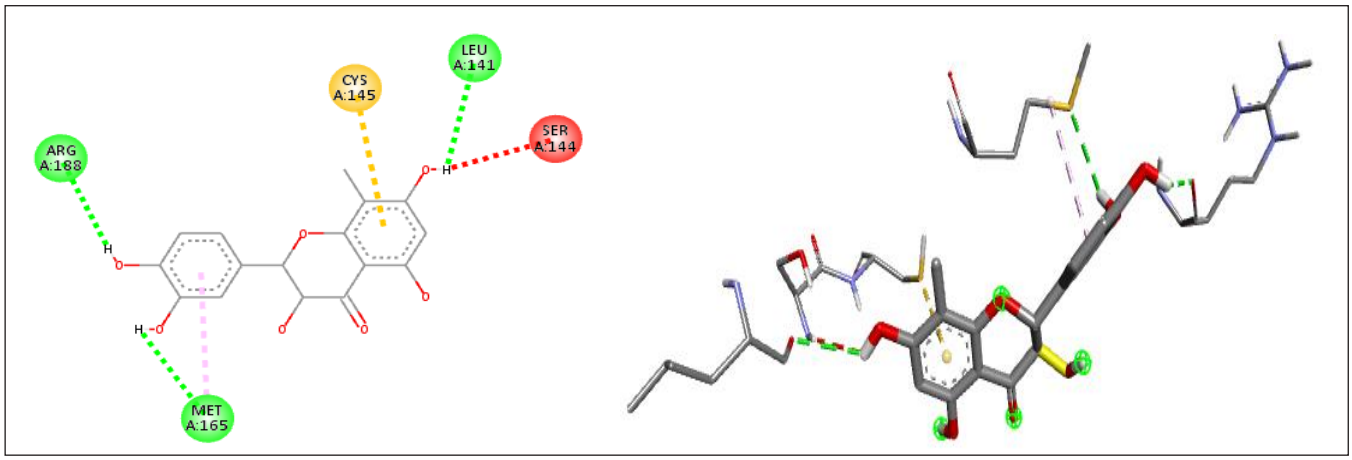

Fig. 7: 2D and 3D interactions of deodarin with main protease (7BUY)

7BUY-cedeodarin, and 7BUY-favipiravir systems were analyzed. The RMSF values for these systems are presented in Table VI. The RMSF plot reveals that the remnants in the α helix and β sheet regions remained relatively stable around 50 ns simulation period. The average RMSF values for 7BUY-quercetin, 7BUY-cedeodarin, and 7BUY-favipiravir were determined to be 0.1426 nm, 0.1730 nm and 0.1508 nm, respectively, as shown in Table VI. This indicates that these compounds exhibit minimal fluctuations in these regions during the simulation.

To evaluate the importance of the chemicals on the concision of the protein, the radius of gyration (Rg) was measured. Table VII presents the Rg values for 7BUY-quercetin, 7BUY-cedeodarin and 7BUY-favipiravir. It was observed that the mean Rg values for 7BUY-quercetin, 7BUY-cedeodarin and 7BUY-favipiravir were 2.192 nm, 2.214 nm, and 2.191 nm, respectively. Notable variations were observed prior to the 50 ns mark in entire simulations, signifying that the ligands tightly bound to the active location and kept the stability of the protein structure (Table VII).

Table VI: RMSF values of 7BUY-quercetin, 7BUY-cedeodarin, and 7BUY-favipiravir

Time (ns)	RMSD (nm)		
	Quercetin	Cedeodarin	Favipiravir
1	0.1426	0.173	0.1508
5	0.1107	0.1155	0.1159
10	0.0715	0.159	0.0789
15	0.0558	0.0787	0.0298
20	0.0482	0.0832	0.0516
25	0.0675	0.0575	0.0662
30	0.0518	0.0606	0.0627
35	0.0608	0.0555	0.0714
40	0.0486	0.0718	0.0593
45	0.0541	0.0797	0.0599
50	0.0405	0.1252	0.0424

Table VII: Rg values of 7BUY-quercetin, 7BUY-cedeodarin, and 7BUY-favipiravir

Time (ns)	Quercetin	Cedeodarin	Favipiravir
	Rg (nm)		
0	2.19264	2.21482	2.19107
10	2.2208	2.2474	2.20906
20	2.22325	2.26326	2.21861
30	2.22931	2.24878	2.22482
40	2.21985	2.25363	2.23154
50	2.22772	2.25821	2.24007
60	2.22371	2.25795	2.23428
70	2.23147	2.26007	2.23758
80	2.21143	2.2536	2.23628
90	2.20147	2.26929	2.23111
100	2.21854	2.2544	2.24543

The protein-ligand aggregates were analyzed for hydrogen-bonding interrelation, as illustrated in Fig. 8. The hydrogen-bonding interactions within the 7BUY-quercetin, 7BUY-cedeodarin and 7BUY-favipiravir complexes were examined based on the 50 ns MD simulations. The 7BUY-quercetin complex displayed 3 hydrogen bonds, the 7BUY-cedeodarin complex had 6 hydrogen bonds and the 7BUY-favipiravir complex exhibited 8 hydrogen bonds. These findings indicate the presence of robust bonding interactions within the protein-ligand complexes (Fig. 8).

DISCUSSION

Coronaviruses have been associated with various disorders affecting the gastrointestinal, urinary, hepatic, and central nervous systems in both humans and animals over a significant period of time. The advent of SARS-CoV-2, the virus accountable for the continuing COVID-19 pandemic, poses substantial health risks to humans[30]. Managing this viral infection has primarily focused on clinical interventions, such as infection prevention, protective steps and supportive attention. Presently, no precise clinical therapies are accessible for SARS-CoV-2 virus. Therefore, the identification and development of new potential drug candidates are essential in mitigating the health impact caused by SARS-CoV-2 and combating the continuing pandemic.

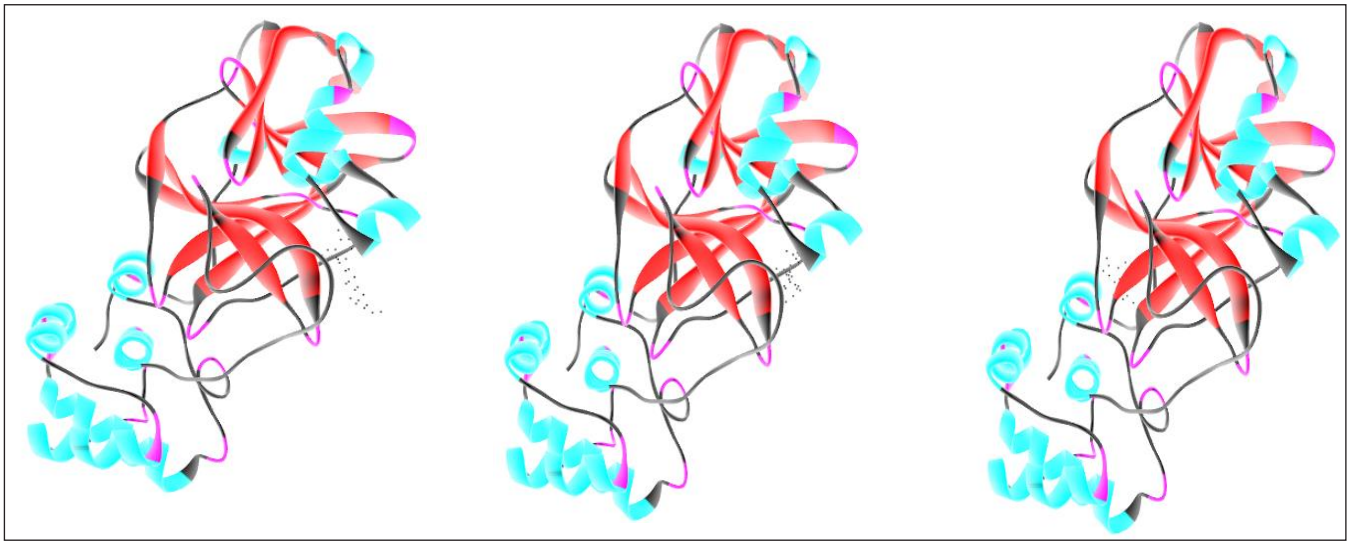

Fig. 8: Complex structures of 7BUY-quercetin, 7BUY-cedeodarin, and 7BUY-favipiravir

The discovery of the main protease (M^{Pro}) in COVID-19 has furnished an awesome chance to explore potential therapeutic options against corona viruses. Natural compounds have gained attention in recent years as promising antiviral treatments[31]. Given the urgent need for COVID-19 therapies and the potential of naturally derived compounds in drug development, we conducted a screening of phytochemical constituents from *C. deodara*. This screening aimed to identify potential compounds that could be utilized in the production of medicines for COVID-19.

The current study has the potential to identify or enhance a potential lead compound for further experimental investigations. Our research primarily aimed to evaluate the *in silico* efficacy of specific key phytochemical constituents derived from the medicinal plant *C. deodara* against COVID-19. Based on the docking results, two phytochemicals from *C. deodara* were specifically selected for additional molecular dynamics research[32]. This further investigation were expected to provide valuable insights into the behavior and interactions of these compounds, paving the way for potential therapeutic advancements in the fight against COVID-19.

Out of the 53 possibilities examined, three substances demonstrated a higher binding affinity and required less energy to bind to the primary protease. Quercetin exhibited a minimum binding energy of approximately 7.2 kcal mol^{-1} when interacting with the primary protease. It formed 4 hydrogen bonds with ASN A:142, GLY A:143, SER A:144, and CYS A:145, as well as 1 hydrophobic interrelation with MET A:49. Dihydrodehydrodiconiferyl alcohol formed 5 hydrogen bonds with LEU A:141, GLY A:143, SER A:144, CYS A:145, and GLN A:192. Additionally, it had 2 hydrophobic interactions with HIS A:41 and MET A:49, as well as 1 sulfur bond with MET A:165. Cedeodarin established two hydrogen bonds with ARG A:188 and GLN A:192, two hydrophobic interactions with MET A:49 and MET A:165, and one sulfur bond with CYS A:145. These findings indicate strong and specific interactions between these substances and the primary protease.

An interesting correlation between the molecular weight of the chemicals and the docking outcomes was observed in the work. However, it is worth noting that the numeral of chemicals used in the investigation was relatively small, and their molecular weights did not exhibit a wide range of variation. The molecular weights of the three substances—quercetin, dihydrodehydrodiconiferyl alcohol, and cedeodarin are 302.24 g mol^{-1}, 360.40 g mol^{-1}, and 318.28 g mol^{-1}, respectively. Despite the limited range in molecular weights, all three substances demonstrated a strong binding affinity[33]. Furthermore, quercetin and cedeodarin displayed stability in molecular dynamics simulations conducted against the major protease protein. These findings suggest the potential importance of molecular weight and stability in determining the binding affinity and efficacy of these substances.

Based on the research findings, it is evident that the functional pockets of the taunt proteins have the capacity to hold substantial compounds. Still, in order to fully comprehend the relationship between the molecular weight of substances and their conformation, additional experimental data is required. Experimental validation will provide more insights into the impact of molecular weight on the binding affinity and effectiveness of the identified substances[34].

The Lipinski's Rule of Five serves as a fundamental guideline for assessing drug likeliness. It defines certain molecular characteristics, including ADME (absorption, distribution, metabolism, and excretion), that are essential for understanding the pharmacokinetics of drugs in human. Lipinski's rule outlines specific requirements for optimum drug candidates. Despite being derived from natural sources, the top three compounds with the highest scores in our study did not adhere to Lipinski's criteria. However, the ADME predictions for these selected three compounds passed the ADME check screens, indicating favorable properties in terms of absorption, distribution, metabolism, and excretion[35].

Based on the MD simulation calculations, the complexes 7BUY-quercetin, 7BUY-cedeodarin, and 7BUY-favipiravir have been identified as possible *in silico* inhibitors for the appropriate target proteins. These findings from the preliminary investigation of potential anti-viral compounds will play a crucial role in informing and guiding future experimental research contrary to SARS-CoV-2 (COVID-19). The outcomes provide valuable insights and serve as a starting point for further exploration and development of these compounds as potential treatments for the disease.

CONCLUSION

In this study, various bioinformatics tools, including admetSAR, Autodock, GROMACS, and PASS analysis, were utilized to identify possible compounds from *C. deodara* that could target the primary protease of COVID-19. The results of the present work indicate that quercetin and cedeodarin, two phytoconstituents from *C. deodara*, show promise as potential inhibitors of the COVID-19 major protease. These findings suggest that further investigations in *in vitro* and pre-clinical settings are warranted to evaluate the efficacy of quercetin and cedeodarin as potential treatments for COVID-19.

REFERENCES

1. World Health Organization. Coronavirus disease 2019 (COVID19): Situation report. 2020, 70.
2. Shaik A., and Atmakuri L.R.: Clinical trials status and approaches of COVID-19 vaccines developed globally: The Recent Updates. **Pharma Times,** 2022, 54(3), 7-14.
3. Rouchka E.C., Chariker J.H. and Chung D.: Phylogenetic and variant analysis of 1,040 SARS-CoV-2 Genomes. 2020
4. Lu R., Zhao X. and Li J.: Genomic characterization and epidemiology of 2019 novel coronavirus: implications for virus origins and receptor binding. **Lancet,** 2020, 395, 565-574.
5. Jin Z., Du X. and Xu Y.: Structure of Mpro from COVID-19 virus and discovery of its inhibitors. bioRxiv. Preprint. 2020
6. Hui D.S., Azhar E.I. and Madani T.A.: The continuing 2019-nCoV epidemic threat of novel coronaviruses to global health - The latest 2019 novel coronavirus outbreak in Wuhan, China. **Int. J. Infect. Dis.,** 2020, 91, 264-266.
7. Moses T. and Goossens A.: Plants for human health: greening biotechnology and synthetic biology. **J. Exp. Bot.,** 2017, 68, 4009-4011.
8. Schaal B.: Plants and people: our shared history and future. **Plants People Planet,** 2019, 1, 14-19.
9. Jassim S.A.A. and Naji M. A.: Novel antiviral agents: a medicinal plant perspective. **J. Appl. Microbiol.,** 2003, 95, 412-427.
10. Hussain W., Haleem K.S. and Khan I.: Medicinal plants: a repository of antiviral metabolites. **Future Virol.,** 2017, 12, 299-308.
11. Shaik A., Atmakuri L.R. and Maram C.E.: *In vivo* antioxidant activity of different fractions of *Indigofera barberi* against paracetamol induced toxicity in rats. **Turk. J. Pharm. Sci.,** 2020, 17(2), 136-140.
12. Chaudhuri S., Symons J.A. and Deval J.: Innovation and trends in the development and approval of antiviral medicines: 1987-2017 and beyond. **Antivir. Res.,** 2018, 155, 76-88.
13. Sander T., Freyss J. and Von Korff M.: Datawarrior: an open-source program for chemistry aware data visualization and analysis. **J. Chem. Inf. Model,** 2015, 55, 460-473.
14. Sussman J.L., Lin D. and Jiang J.: Protein Data Bank (PDB): database of three-dimensional structural information of biological macromolecules. **Acta Crystallogr. D Biol. Crystallogr.,** 1998, 54, 1078-1084.
15. Aminabee S.K., Raveesha P., Adithya V., Mohansai M., Shaherbanu, Harshitha K., Himaja Kasthuri K., Lakshmi Priya M., Chandini Naga Mallika G. and Lakshmana Rao A.: *In vivo* antinociceptive activity and *In silico* molecular docking of selected phytoconstituents of methanolic extract of *Hypericum japonicum*. **J. Drug Alcohol Res.,** 2022, 11(5), 01-08.
16. Kar P., Sharma N.R. and Singh B.: Natural compounds from *Clerodendrum* spp. as possible therapeutic candidates against SARS-CoV-2: An *in silico* investigation. **J Biomol. Struct. Dyn.,** 2020, 1-12.
17. Morris G.M., Huey R. and Lindstrom W.: Autodock4 and AutoDockTools4: Automated docking with selective receptor flexibility. **J. Comput. Chem.,** 2009, 30, 2785-2791.
18. O'Boyle N.M., Banck M. and James C.A. Open Babel: an open chemical toolbox. **J Cheminform.,** 2011, 3, 33.
19. Pangastuti A., Amin I. F. and Amin A.Z.: Natural bioactive compound from *Moringa oleifera* against cancer based on *in silico* screening. **J. Teknol.,** 2016, 78, 315-318.
20. Prasanth D.S.N.B.K., Aminabee S.K., Lakshmana Rao A., Guntupalli Ch., Rajasekhar Reddy A., Umasankar K., Koteswara Rao S.N., Rajeshwari P.: Inhibitory effects of *Manosa alliacea* in Freund's adjuvant arthritis on inflammatory markers and its confirmation by *In silico* strategy. **Thai J. Pharm. Sci.,** 2021, 45(6), 532-544.
21. Seeliger D. and De Groot B.L.: Ligand docking and binding site analysis with PyMOL and Autodock/Vina. **J. Comput. Aided Mol. Des.,** 2010, 24, 417-422.
22. Yang H., Lou C. and Sun L.: AdmetSAR 2.0: Web-service for prediction and optimization of chemical ADMET properties. **Bioinformatics,** 2019, 35, 1067-1069.
23. Cheng F., Li W. and Zhou Y.: AdmetSAR: A comprehensive source and free tool for assessment of chemical ADMET properties. **J. Chem. Inf. Model.,** 2012, 52, 3099-3105.

24. Khurana N., Ishar M.P.S. and Gajbhiye A.: PASS assisted prediction and pharmacological evaluation of novel nicotinic analogs for nootropic activity in mice. **Eur. J. Pharmacol.,** 2011, 662, 22-30.
25. Mittal M., Goel R.K. and Bhargava G.: PASS-assisted exploration of antidepressant activity of 1,3,4-trisubstituted-β-lactam derivatives. **Bioorg. Med. Chem. Lett.,** 2008, 18, 5347-5349.
26. Goel R.K., Singh D. and Lagunin A.: PASS-assisted exploration of new therapeutic potential of natural products. **Med. Chem. Res.,** 2011, 20, 1509-1514.
27. Van Der Spoel D., Lindahl E. and Hess B.: GROMACS: fast, flexible, and free. **J. Comput. Chem.,** 2005, 26, 1701-1718.
28. Gangadharappa B.S., Sharath R. and Revanasiddappa P.D.: Structural insights of metallo-beta-lactamase revealed an effective way of inhibition of enzyme by natural inhibitors. **J. Biomol. Struct. Dyn.,** 2020, 38, 3757-3771.
29. Chandramohan V., Kaphle A. and Chekuri M.: Evaluating andrographolide as a potent inhibitor of NS3-4A protease and its drug resistant mutants using *in silico* approaches. **Adv. Virol.,** 2015, 15, 20-67.
30. Prasanth D.S.N.B.K., Aminabee S.K., Lakshmana Rao A., Teja N., Bhargavi K., Monika Ch., Pujitha B., Sandhya T., Lalitha A. and Siva Prasad P.: Antihelmintic activity of *Mansoa alliacea* against *Pheretima posthuma*: *In vitro* and *In silic*o approach. **Thai J. Pharm. Sci.,** 2020, 44(3), 86-196.
31. To K.K., Hung I.F. and Chan J.F.: From SARS coronavirus to novel animal and human coronaviruses. **J. Thorac. Dis.,** 2013, 5(2), S103-S108.
32. Zhu N., Zhang D. and Wang W.: A novel coronavirus from patients with pneumonia in China, 2019. **New Engl. J. Med.,** 2020, 82, 727-733.
33. Zhou Y., Hou Y. and Shen J.: Network-based drug repurposing for novel coronavirus 2019-nCoV/SARS-CoV-2. **Cell Discov.,** 2020, 6, 14.
34. Lin L.T., Hsu W.C. and Lin C.C.: Antiviral natural products and herbal medicines. **J. Tradit. Complem. Med.,** 2014, 4, 24-35.
35. Martinez J.P., Sasse F. and Bronstrup M.: Antiviral drug discovery: broad-spectrum drugs from nature. **Nat. Prod. Rep.,** 2015, 32, 29-48.